INTERNATIONAL
Agrophysics
www.international-agrophysics.org

Int. Agrophys., 2024, 38, 447-456
doi: 10.31545/intagr/194769

Old and new wetting liquids separation in grain-based pattern micromodel during wetting cycles**

Qun-Zhan Huang[1], *Shao-Yiu Hsu*[1]*, *Hsiang Chen*[2], *Chia-Wen Tsao*[3], *Krzysztof Lamorski*[4], *Cezary Sławiński*[4]

[1]Department of Bioenvironmental Systems Engineering, National Taiwan University, No. 1, Sec. 4, Roosevelt Rd., Taipei 106319, Taiwan (R.O.C.)
[2]Graduate Institute of Hydrological and Oceanic Sciences, National Central University, No.300, Jhongda Rd., Jhongli City, Taoyuan County 320, Taiwan (R.O.C)
[3]Department of Mechanical Engineering, National Central University, No.300, Jhongda Rd., Jhongli City, Taoyuan County 320, Taiwan (R.O.C)
[4]Institute of Agrophysics, Polish Academy of Sciences, Doświadczalna 4, 20-290 Lublin, Poland

Received August 1, 2024; accepted October 16, 2024

Abstract. In soils, old (residual) water can persist despite new (invading) water infiltration, potentially due to trapped air bubbles isolating old water pockets. However, the mechanisms behind air bubble formation and liquid separation remain unclear. This study aims to investigate the interaction between new and old wetting liquids and the mechanism that traps air bubbles, isolating old water. Using a grain-based pattern micromodel, we examined these processes during a repeated wetting cycle (wetting-drainage-evaporation-wetting). To enhance visualization and evaporation, we used dyed alcohol solutions as the wetting phase, with air as the non-wetting phase. Results indicate that a liquid film on grains plays a crucial role in old liquid entrapment, influenced more by soil wettability than initial liquid content. Strong wettability resulted in significant film development, allowing old and new liquids to connect and potentially mix. In contrast, weak wettability led to air bubble entrapment, isolating old water and preventing its displacement. The findings highlight that soil wettability and wetting film development are key factors in the interaction between new and old wetting liquids.

Keywords: wetting phase entrapment, grain-based pattern micromodel, newold water interaction, ecohydrological separation

1. INTRODUCTION

Field hydro-isotopic measurements suggest an ecohydrological separation between plant uptake and soil water drainage, indicating a distinction between subsurface pore waters that originate from different rainfall events (Berkowitz, 2014; Brooks *et al*., 2010; Finkenbiner *et al*., 2022; Gouet-Kaplan and Berkowitz, 2011; Gouet-Kaplan *et al*., 2009; Oerter and Bowen, 2017). Instead of being fully displaced by event water (events such as rainfall or irrigation), pre-event water could be partially mixed with event water. Drying old water through evaporation is important because it causes old water pockets to reside in small pores, making them less easily replaced or mixed with new water (Huang *et al*., 2023). In addition to ecohydrological separation, interaction between soil waters influences the water components and quality of streams and groundwater, as well as the nutrients taken up by plants.

These interaction mechanisms are typically categorised as matrix and preferential flows at a macroscopic level. Sklash *et al*. (1986) and Kirchner *et al*. (2000) observed in field studies that when matrix flow dominates the subsurface

*Corresponding author e-mail: syhsu@ntu.edu.tw
**This work was funded by National Science and Technology Council under grant: NSTC 113-2116-M-002-001- (2024-2025).

flow process, stored water is replaced by invading water and is first discharged into streams or groundwater. Sklash *et al*. (1986) observed that soil water runoff was first contributed by pre-event water and later by the event water. Kirchner *et al*. (2000) reported an initially high contamination streamflow after a rainfall event. In contrast, when preferential flows (*e.g*. macropore and pipe flows) dominate the subsurface flow, the event water contributes to the groundwater or streamflow earlier than expected by matrix flow. For instance, a tracer test conducted by Turton *et al*. (1995) employing a series of artificial rainfall cycles indicated that macropore flows likely dominated the experiment because the ratio of subsurface flow contributed by water from the first rainfall cycle increased after the rainfall had stopped. The dominance of matrix and macropore flows is related to rainfall intensity and soil wetness (Radolinski *et al*., 2021; Uchida *et al*., 2005). Comparing hillslope surveys, Uchida *et al*. (2005) found that measurable pipe flow occurs when the total rainfall amount exceeds a threshold associated with the pre-storm wetness. Radolinski *et al*. (2021) conducted pot experiments, finding that rainwater contributes to soil discharge at an early stage when rainfall intensity is sufficiently high. In addition, the initial soil water content influences the path of the invading water. For example, sand column experiments conducted by Horton and Hawkins (1965) showed that rainwater preferentially flows along paths wetted by retained water at field capacity.

However, according to Finkenbiner *et al*. (2022), eco-hydrological separation is unlikely to be explained solely by conventional soil physics. As micromodel experiments provide straightforward results for new and old water interactions, investigating the interplay between event and pre-event liquids at a pore scale, rather than at the Darcy scale, could help reveal the mechanisms involved.

Using cyclic infiltration micromodel experiments, Gouet-Kaplan and Berkowitz (2011) observed that new water notably replaces the original pore water during the early stage of a first wetting event. Afterwards, the interplay reaches a stable state where the main pathways are formed for the invading water. This result is consistent with the results of sandbox experiments conducted by Gouet-Kaplan *et al*. (2009), in which the yielded water was initially primarily old water. The ratio of old water to yielded water decreases and eventually stabilises. The nonwetting phase (*e.g*. air in soil) trapped in porous media aids in the separation (Huang *et al*., 2023; Wang *et al*., 2023). Huang *et al*. (2023) demonstrated the importance of air bubble entrapment in new- and old-water interactions using pore doublet micromodel experiments. Trapped air bubbles for separating the new and old wetting liquids were accomplished by pre-shrinking the original residual wetting liquid (old liquid) through evaporation, which reduced the likelihood of the new invading wetting liquid coming in contact with the old liquid. However, the films developing around the trapped air bubbles provided an unexpected connection between the new and old liquids. Nevertheless, the pore doublet micromodel used by Huang *et al*. (2023) considerably simplified the pore geometry compared with that of real soil or sand-packed samples. The mechanisms underlying the formation of trapped air bubbles that separate the new and old liquids remain unclear.

In this study, experiments were conducted using grain-based micromodels. The channel pattern was designed based on an X-ray CT scanning slice of a quartz-sand-packed sample. With this pore geometry, we aimed to investigate the interaction between new and old wetting liquids and the mechanism that facilitates trapping air bubbles and isolating the old wetting liquid pockets during repeated wetting cycles. The wetting-drainage-evaporation-wetting process is analogous to a rainfall-dry-season-rainfall cycle. Based on information from Huang *et al*. (2023), we initially expected that the initial old liquid content before the invasion of new liquid could be important. Accordingly, we conducted experiments with different initial old liquid contents through the evaporation step. To accelerate the evaporation and visualisation experiments, the wetting phase was dyed alcohol solutions, and the nonwetting phase was air.

2. METHOD

2.1. Fabrication of grain-based micromodel

Figure 1a shows the micromodel design. The central 1 × 1 cm^2 region represents the porous medium of interest. The left and right channels represent the inlet and outlet channels, respectively. The pore pattern (Fig. 1a) was designed based on an X-ray slice of a medium-grain quartz-sand-packed sample obtained using X-ray microcomputed tomography scan (Lamorski, 2017). However, the image

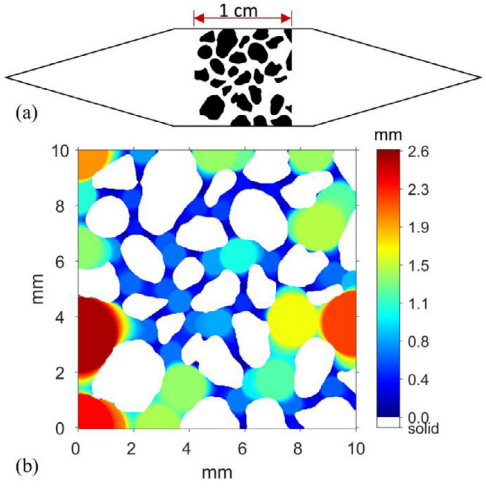

Fig. 1. Grain-based micromodel. (a) Design of the grain-based micromodel. The white portion represents the channel, and the black areas represent the grains. (b) Pore sizes in the central 1 × 1 cm^2 region. The sizes are calculated based on continuous open operation.

was scaled because of our fabrication limitations. Fig. 1b shows the pore size of the channel pattern during continuous open operation (Liu and Jeng, 2019).

We fabricated several micromodels with the same design. The micromodels were fabricated using a regular polydimethylsiloxane (PDMS) modelling process (Shao *et al*., 2012) with a master mold. The master mold contained the pattern of the designed channel, which was transferred onto a PDMS piece after PDMS modelling. The master mold was microfabricated using UV lithography (AGL100 UV Light source; M&R Nano Technology Co., Taoyuan, Taiwan) (Hsu *et al*., 2017). After transferring the pattern onto a PDMS piece, we perforated the inlet and outlet holes to inject fluid into the micromodel. This piece was covered and bonded to a flat PDMS piece to close the channel. Before closing the channel, an oxidising plasma treatment (Plasma Cleaner PDC-32G, Harrick Plasma Inc., New York, USA) was applied to the bonded surfaces of the two PDMS pieces. This treatment enhances the bonding effect (Chaudhury and Whitesides, 1991, 1992; Shao *et al*., 2012). The channel depth of the micromodel was 100 μm. The pore area in the central 1 × 1 cm^2 region was 0.55 cm^2.

2.2. Experimental setup and process

We conducted wetting-drainage-evaporation-wetting experiments. The wetting phase comprised a 95% alcohol solution and a dyed alcohol solution (with blue food dye), whereas the nonwetting phase was air. In the air-alcohol-PDMS system, the contact angle was approximately 30°, estimated by the sessile drop method. Figure 2 shows the experimental setup and steps. As Fig. 2a shows, a syringe pump (LEGATO 200, KD Scientific Corp., Massachusetts, USA) was used to inject fluids into the micromodel. The experiments were recorded using a digital camera (GS3-U3 41C6C; Point Grey Research, Inc., Canada).

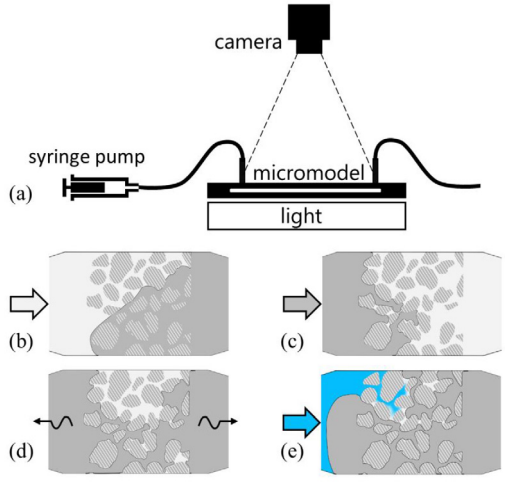

Fig. 2. Schematic of experimental (a) setup and steps, (b) first wetting, (c) drainage (injecting air), (d) evaporation, (e), and (f) second wetting with dyed alcohol solution.

During the first wetting step (Fig. 2b), the 95% alcohol solution saturated the model at an injection rate of 3 μL min^{-1}, followed by drainage using injected air at the same injection rate (Fig. 2c). During the evaporation step (Fig. 2d), the alcohol solution decreased because of evaporation. In the second wetting step (Fig. 2e), the dyed new alcohol solution was also injected at 3 μL min^{-1}. We performed four experiments, A, B, C, and D, with evaporation times of 32, 39, 50, and 73 min, respectively.

2.3. Image segmentation of air, liquid, and grain regions

The experiment images were RGB images: colored images where each pixel is represented by three values (Red, Green, Blue), each ranging from 0 to 255. Principal component analysis (PCA) was conducted to transform the image into a colour coordinate system, in which the air, liquid, and grain regions exhibited maximum differences. Initially, we selected a training m × RGB image (Fig. 3a) containing the pure invading liquid, original remaining liquid, and air. This training image was used to calculate the matrix of principal component coefficients (W, a 3-by-3 orthogonal matrix), and the estimated means (μ_1, μ_2, and μ_3) of the R (red), G (green), and B (blue) component.

To perform PCA, the training image (m × n × 3 matrix) was converted into an mn-by-3 matrix X_0. Each row of X_0 represents the values of the R, G, and B components of a pixel. With X_0, we calculated W, μ_1, μ_2, and μ_3 from the training image. Subsequently, X_0 was projected onto the PCA space using the following equation:

$$Y = (X_0 - [\mu_1 J, \mu_2 J, \mu_3 J])\, W,$$

where: J is an mn-by-1 matrix of ones.

A similar process was followed for the other experimental images. Each RGB image was reshaped into an mn-by-3 matrix X. Matrix X was projected onto the PCA space in terms of Y by substituting X for X_0 in the above equation. After reshaping each column of Y into an m × n matrix, the images of each principal component were obtained.

Figure 3 shows an example of the image-processing procedure. The air, liquid, and solid regions in Fig. 3a were identified manually, as shown in Fig. 3b-e show the images of each principal component. As shown in Fig. 3c, the air regions are identified by examining whether the values of the first component (Y_1) exceed a specified threshold (th_1). As Fig. 3d shows, the air regions are identified by examining whether the values of the second component (Y_2) fall below a specified threshold (th_2). Thresholds th_1 and th_2, were determined manually. However, as shown in Fig. 3e, the air, liquid, and solid regions could not be distinguished.

Accordingly, after calculating the Y_1 and Y_2 for an experiment image using W, μ_1, μ_2, and μ_3, the air region could be determined preliminarily by checking whether both conditions $Y_1 > th_1$ and $Y_2 < th_2$ were met. Next, the solid region was preset directly because it was known. The remaining region was classified as liquid. Additionally, the saturation

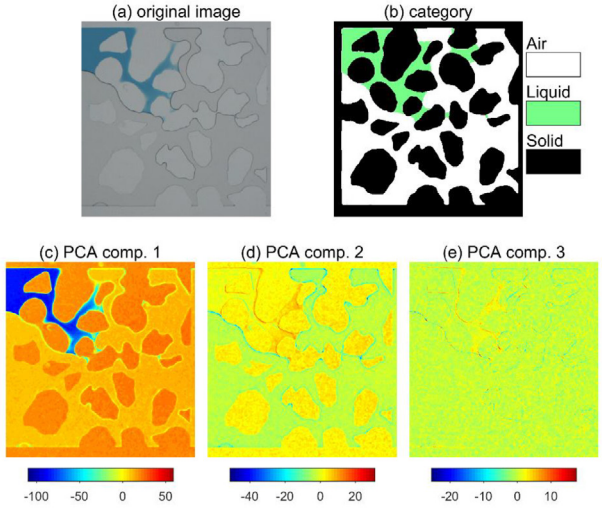

Fig. 3. Classification of air, liquid, and grain regions: (a) example image, (b) image showing liquid, air, and solid categories. The area marked in black represents the grain and part of the region outside the area of interest, (c) to (d) demonstrate the images of each PCA component.

of air (S_{air}) and liquid (S_{liquid}) were calculated by dividing the area (pixels) by the pore area (pixels). Although S_{liquid} was underestimated owing to the difficulty of removing noise and identifying wetting films, the segmentation process could still identify the major regions of the liquid.

2.4. Estimation of new and old liquid amounts during the second wetting step

A dense dye concentration resulted in a high colour saturation in the hue-saturation-value (HSV) system (Fig. 3a and Fig. 4). Therefore, in this study, the relative concentration of the dye solution was determined by normalising the colour saturation between 0 and 100%, where 0% refers to the new liquid, and 100% to the pure old liquid. The normalised colour saturation was denoted S_C.

The average S_C of the liquid area was calculated for each image. The average S_C are values were denoted $\overline{S}_C$. A high $\overline{S}_C$ indicates a high ratio of invading liquids occupying the liquid area. A low $\overline{S}_C$ should result from the old liquid remaining in the micromodel. Therefore, we quantified the relative content of new liquid (S_{new}) in the pore channel using $S_{liquid}\,\overline{S}_C$. The old liquid saturation (S_{old}) was estimated by $S_{liquid}\,(1 - \overline{S}_C)$.

3. RESULTS AND DISCUSSIONS

3.1. Initial old liquid after the evaporation step

In the drainage step, because the grains were located loosely in the lower part of the micromodels (Fig. 1b), air penetrated the micromodels through the paths in this region (Fig. 5a-d). The differences in these initial S_{liquid} values derived from minor structural differences between the microfluidic devices.

At the beginning of the second wetting step, the initial S_{liquid} values in experiments A, B, C, and D were approximately 10, 11, 15, and 17%, respectively. The initial S_{liquid} values were calculated from Fig. 5e-h. After drainage, the micromodels were dried for different periods. However, the changes in S_{liquid} values after drying were not proportional to the applied evaporation times because the distributions and amounts of old liquids in the micromodels differed after the drainage step (Fig. 5a-d). In experiment A, some of the grains were coated with wetting films after evaporation

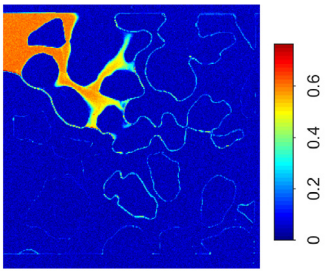

Fig. 4. Saturation of colour for Fig. 3a.

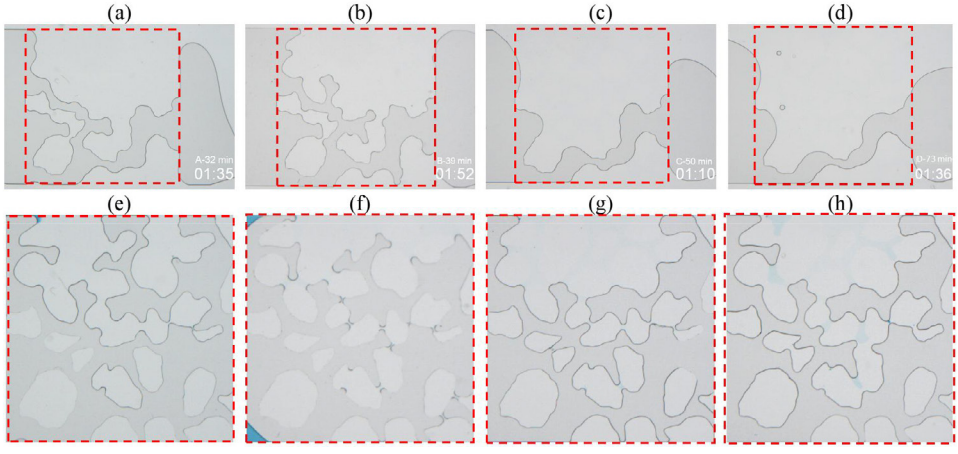

Fig. 5. Experimental images at (a-d) the end of the drainage step, and (e-h) the beginning of the second wetting step. The time, *e.g.* 01:35, 01:52 in (a-d) indicates the air injection time. Subfigures (a) and (e) are from experiment A, (b) and (f) are from experiment B, (c) and (g) are from experiment C, and (d) and (h) are from experiment D. The dashed box indicates the central porous area.

(Fig. 5e), whereas in experiment B, despite having a similar initial S_{liquid} to that in experiment A, only a few of the grains were covered by wetting films (Fig. 5f). In contrast, in experiments C and D, the initial S_{liquid} values were higher than those in experiments A and B, and the wetting films coated most of the grains (Fig. 5g, h).

3.2. Old liquid during the second wetting step

Figures 6-9 show the evolution of fluid saturation during the second wetting step with our classification approach. With additional liquid injected into the micromodel, S_{liquid} increased, whereas S_{air} decreased in each experiment. With an injection rate of 3 μL min^{-1}, the pore volume (5.5 μL) was reached after approximately 1.8 min.

During the first 1.8 min, the increase in S_{new} did not rapidly reduce S_{old}, although S_{old} also changed owing to mixing of the new and old liquids. In all the experiments, the old liquid was primarily located in the upper-right region, as shown in Fig. 6b, Fig. 7b, Fig. 8b, and Fig. 9b. However, after 1.8 min, S_{old} decreased in all experiments, except experiment B. In experiment B, the change in S_{old} was limited (Fig. 7d), and a significant amount of the pure old liquid did not mix with the new liquid because of trapped air bubbles (Fig. 7b). In other experiments, only a few (or none) air bubbles were trapped, and the old liquid was mixed with or displaced by the new liquid.

The S_C images after continuous injection of the new liquid for more than 5 min in experiments A, B, C, and D are shown in Fig. 6c, Fig. 7c, Fig. 8c, and Fig. 9c, respectively. The 5 min injection time represents the volume of the injected new fluid, which was more than three times the

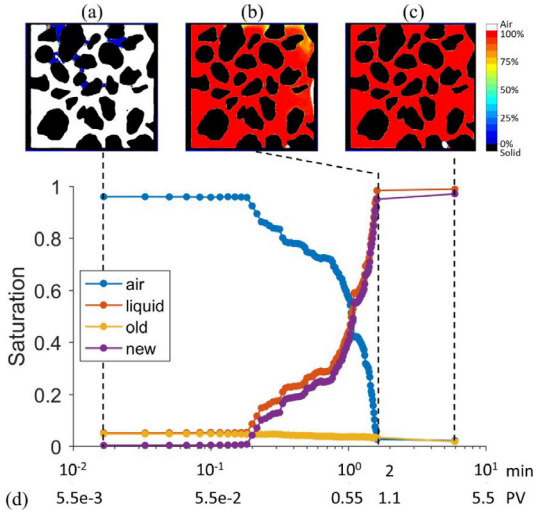

Fig. 6. Relative new liquid concentration mapping (S_C) and saturation of fluids in experiment A during the second wetting step. Subfigures (a-c) demonstrate S_C, with its value indicated by the colour bar. Subfigure d shows the saturations. The dashed lines in subfigure (d) indicate the time points for subfigures (a-c), min means injection duration in minutes. PV means the ratio of injected liquid volume to total pore volume.

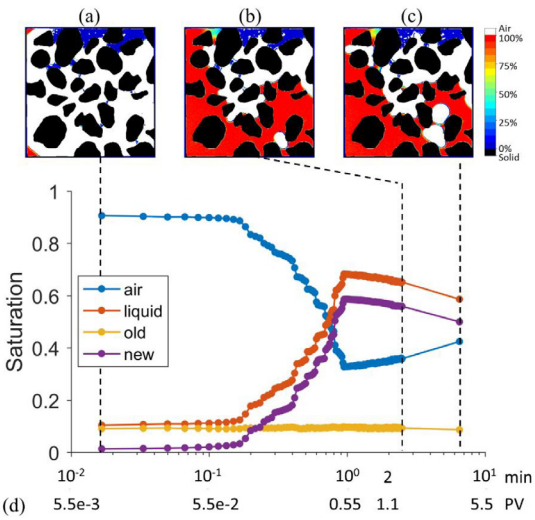

Fig. 7. Relative new liquid concentration mapping (S_C) and saturation of fluids in experiment B during the second wetting step. Subfigures (a-c) demonstrate S_C, with its value indicated by the colour bar. Subfigure (d) shows the saturations. The dashed lines in subfigure (d) indicate the time points for subfigures (a-c), min means injection duration in minutes. PV means the ratio of injected liquid volume to total pore volume.

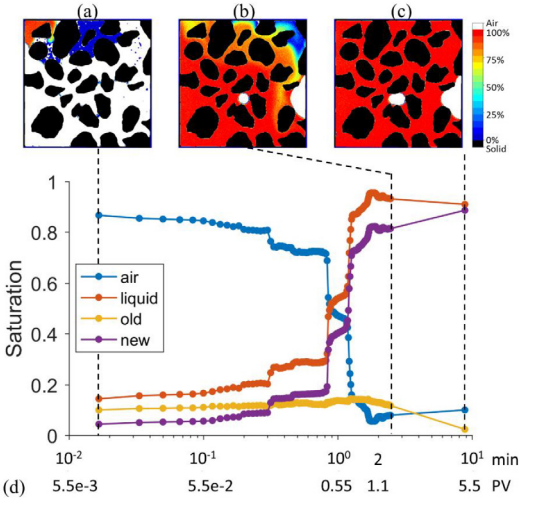

Fig. 8. Relative new liquid concentration mapping (S_C) and saturation of fluids in experiment C during the second wetting step. Subfigures (a-c) demonstrate S_C, with its value indicated by the colour bar. Subfigure d shows the saturations. The dashed lines in subfigure (d) indicate the time points for subfigures (a-c), min means the injection duration in minutes. PV means the ratio of injected liquid volume to total pore volume.

pore volume. Only the S_C image from experiment B consistently showed a significant presence of pure old liquid remaining in the pores. In addition, the trapped air bubbles occupied 30-40% of the pore area (Fig. 7d). Because of the trapped bubbles, some old liquid pockets were trapped in the model, maintaining S_{old} at approximately 9% (Fig. 7d). The slight increase in air saturation in the late stage of the second wetting step was ascribed to the evaporation of the

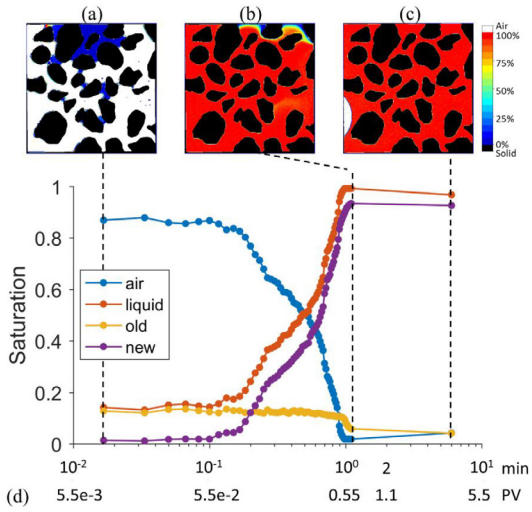

Fig. 9. Relative new liquid concentration mapping (S_C) and saturation of fluids in experiment D during the second wetting step. Subfigures (a-c) demonstrate S_C, with its value indicated by the colour bar. Subfigure d shows the saturations. The dashed lines in subfigure (d) indicate the time points for subfigures (a-c), min means the injection duration in minutes. PV means the ratio of injected liquid volume to total pore volume.

liquid, particularly the new liquid. The new liquid, with a higher alcohol concentration, evaporated more easily than the old liquid.

In experiment A, after injecting a new liquid with more than three times the pore volume, the liquid phase occupied almost the entire channel, with only a small bubble trapped at a dead-end pore (Fig. 6c). The S_{old} value decreased slightly (Fig. 6d). In experiment C, a small air bubble was trapped (Fig. 8c); however, there was a significant reduction in the S_{old} value from 1.8 to 8.8 min (Fig. 8d). In experiment D, no air bubbles were trapped (Fig. 9c). The increase in S_{air} derived from air invading from the inlet. Fig. 9d shows a significant S_{old} reduction.

Additionally, the results of experiments A, C, and D show that when old and new liquids are not separated by air, a portion of the old liquid could be displaced rapidly with the invading liquid passing through. The old liquids in the dead-end pores were not displaced rapidly by the new invading liquid, although the old liquid mixed with and was slowly replaced by the new liquid. As shown in Fig. 6d, Fig. 8d, and Fig. 9d, the liquid areas were nearly fully occupied by the new liquid after more than 5 min of injection.

The results of the interaction between new and old liquids were consistent with the scenario of grains enclosed by wetting films. In experiments A, C, and D, the wetting films enclosed most of the grains at the beginning of the second wetting step, resulting in a new liquid that largely replaced the old liquid. In experiment B, only a few grains were initially covered with wetting films; however, during the second wetting step, air bubbles were trapped, and the new liquid bypassed the region occupied by the old liquid.

3.3. Influences of initial S_{liquid}

Huang *et al*. (2023) conducted pore doublet model experiments, concluding that reducing initial S_{liquid} raises the likelihood of old liquid entrapment. However, in our experimental results, a low initial S_{liquid} did not result in notable old liquid entrapment. The experiments arranged in ascending order of initial S_{liquid} are A, B, C, and D. In experiments A, C, and D, the new liquid was mixed with the old liquid. After injecting more than three times the pore volume of the new liquid, only a small amount of the old liquid remained. In contrast, in experiment B, the entrapped pure old liquid was notable. In addition to the initial S_{liquid}, air bubble entrapment and dead-end pores still significantly prevented the rapid displacement of the old liquid by the invading new liquid (Huang *et al*., 2023; Wang *et al*., 2023).

The different results for old liquid entrapment between experiments A and B are worth noting. Both experiments exhibited similar initial S_{liquid} values; however, only the latter showed a significant amount of pure old liquid. This observation indicates that factors other than the initial S_{liquid} play a crucial role in entrapment of old liquid.

3.4. Differences between experiments A and B

The results of experiments A and B were compared. In the former, the apparent contact angle was approximately 30° (Fig. 10a), and approximately 45° in the latter (Fig. 10b). In experiment B, the ratio of residual old liquid was approximately 9%, and the ratio of trapped air was around 30%. In contrast, these ratios were approximately 2% in experiment A. In addition, the development of wetting films differed between the two experiments. During the first wetting, the film grew in experiment A and was more prevalent than in experiment B (Fig. 10).

The difference in the contact angles between the different experiments was ascribed to the decay of the surface treatment on the PDMS and the concentration of the ethyl alcohol solution (Fan *et al*., 2011; Yu *et al*., 2017). The

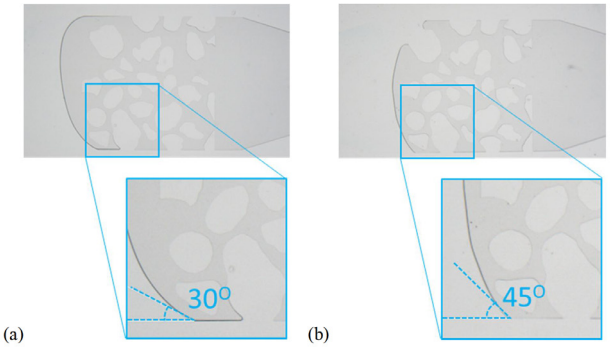

Fig. 10. Apparent contact angles during the first wetting in experiments (a) A and (b) B were 30 and 45°.

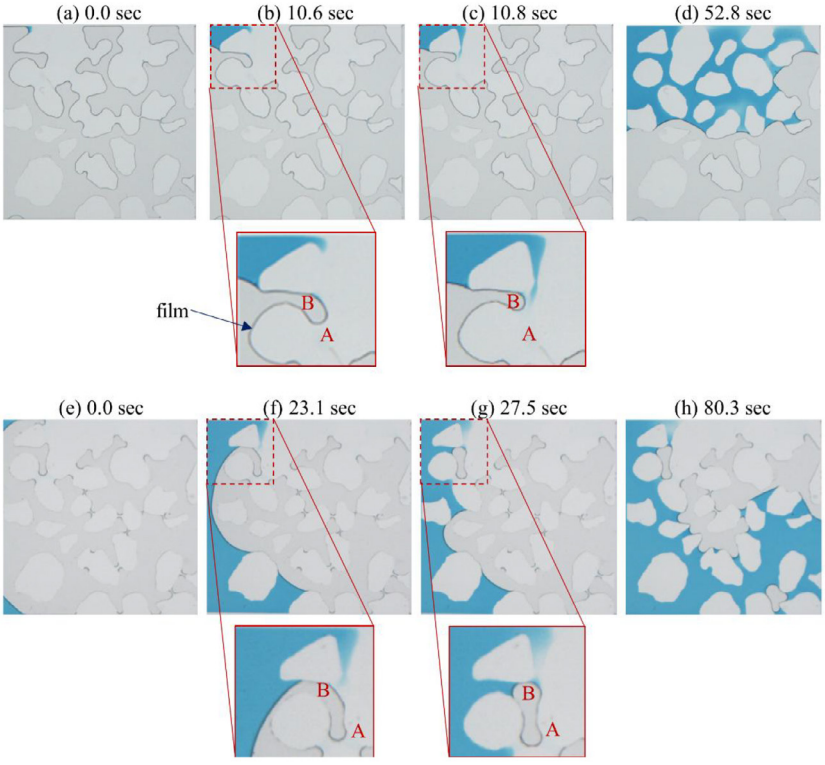

Fig. 11. Images taken during the second wetting step in experiment A (a-d) and experiment B (e-h).

applied surface treatment (oxidising plasma treatment) creates silanol groups on the PDMS surface (Chaudhury and Whitesides, 1991,1992; Shao *et al*., 2012), resulting in the original hydrophobic surface becoming hydrophilic (Bodas and Khan-Malek, 2006; Mata *et al*., 2005). Nevertheless, the concentration decreased as more ethyl alcohol evaporated from the solution and changed the contact angle.

After the drainage step, corner-wetting films were observed in experiments A and B (Fig. 5a, b). Nevertheless, in experiment B, the films split and became piecewise after evaporation (Fig. 11e). In experiment A, as the grains were coated with films (Fig. 11a), the new and old liquids connected easily with each other (Fig. 11b, c). As shown in Fig. 11b and c, the new and old films were connected in the early stage of the second wetting step. In Fig. 11b, c, f, and g, a meniscus is observed (marked A) and a pore body (marked B). Because of the connection, meniscus A moved forward to balance the capillary force and displaced the air between old and new liquids in pore B, with no air bubble being trapped at pore B. In contrast, such a connection did not exist in experiment A, and meniscus A did not connect with the invading liquid and was stagnant at the same place because it lacked a connected liquid film.

3.5. Role of films in interaction of old and new wetting liquids

Similar to that in Huang *et al*. (2023), we found that wetting films notably affected the new and old liquid interactions. Huang *et al*. (2023) indicated that although entrapped bubbles created a barrier between new and old liquids, corner films could serve as paths for new liquid to intrude into the area initially occupied by old liquid.

In our study, at the beginning of the second wetting step in experiments A, C, and D, menisci at different pore throats were connected to each other through films. Under such conditions, the new liquid tended to flow along the original old pockets linked with the wetting films. Therefore, the presence of films reduces the likelihood of old liquid entrapment.

The role of films is illustrated schematically in Fig. 12 for cases with and without film coatings on the grains. Figure 12a shows a wetting phase trapped between two grains coated with films. Once the invading wetting liquid touched the film, the meniscus of the trapped liquid moved because of the capillary force. This movement pushed and displaced air into the pores, thereby preventing the entrapment of air bubbles. Figure 12b shows a wetting liquid trapped between two grains without film coating. When the invading wetting liquid contacted one of the grains, the meniscus of the residual liquid became immobile because

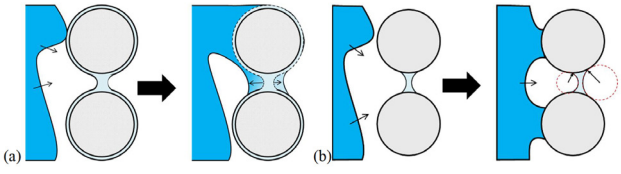

Fig. 12. Schematic of wetting film influence: (a) film coating grains, (b) no film coating on any grains.

no film connected the new and old liquids. Air could not displace the meniscus of the old liquid because the meniscus was immobile, resulting in a higher likelihood of air entrapment. The Jamin Effect (Smith and Crane, 1930) enhances the immobility of air bubbles. Additionally, a slight displacement of the residual liquid increases the capillary force against air bubble penetration through the pore throat (Fig. 12b).

The findings of pore-scale modelling, with connecting pore water being the invading path of new water, reflect the Darcy-scale phenomena found by Horton and Hawkins (1965). The soil column experiments conducted by these authors show that rainwater tends to flow through columns along flow paths that are wetted because of the water retained by the soil at field capacity. Because the soil particles should be covered by water at field capacity, newly invading water has a high chance of encountering the original residual water, which also exhibits high connectivity. Our findings at pore scale indicate that the intrusion of new water changed the pressure head gradient in pre-existing water, immediately triggering movement. This movement led to the flow of new water along the pre-wetted paths.

3.6. Key factors of film development

Our experimental results indicate the importance of wetting films for new and old water interactions. Previous studies have shown that film development was related to wettability and pore geometry (Bico and Quéré, 2003; Concus and Finn, 1969, 1974; Tsao *et al*., 2020). Bico and Quéré (2003) showed that film growth was stronger when a larger capillary difference existed between the tip of the film and its connecting bulk meniscus. For films along the corners of a channel, the capillary difference and growth rate are related to the contact angle (θ) and the geometry of the corner (*e.g*., corner angle α) (Concus and Finn, 1969, 1974; Tsao *et al*., 2020). A small θ results in a robust growth rate as an offset to evaporation. The values $\theta + \alpha/2$ should be less than 90° to result in a film curvature direction towards the inner pore and a negative capillary force drawing the liquid from the bulk meniscus to the corner. In both the old and new liquids in experiment B, the corner film did not spontaneously grow, implying that $\theta + \alpha/2$ could be larger than 90°.

In natural porous media, soil with partial wettability and repellence is common (Dekker *et al*., 2005; Ritsema and Dekker, 2012; Roper *et al*., 2015). Repellent soil is caused when particulate organic matter covers the soil particles (Roper *et al*., 2015) and is related to soil moisture (Doerr and Thomas, 2000). Previously wetted soil can re-establish its water repellence through soil drying (Doerr and Thomas, 2000; Ma'shum and Farmer, 1985; Tschapek, 1984; Valat *et al*., 1991). With weak film development, the experiment with a large apparent contact angle exhibited more air entrapment and resulted in the strong separation of new and old liquids. In addition, repellent soil enhances preferential water flow and irregular wetting patterns (Dekker and Ritsema, 2000). The preferential water flows bypass the pores occupied by old water, similar to that shown in experiment B. Based on the aforementioned mechanism, soil drying could enhance soil repellence and the separation of new and old water.

Particle roundness also influences film development. In drying experiments using micromodels, Geistlinger *et al*. (2019) observed that a film could entirely cover square grains, whereas water surrounding single grains was observed by Vorhauer *et al*. (2015). Geistlinger *et al*. (2019) indicated that grains with sharp corners resulted in unstable films at the corners that snapped off. The grains were round in our micromodels and should have facilitated film development.

In experiment B, several isolated old liquid pockets were separated from the invading liquid during the second wetting process. In real soil, the residual liquid could be disconnected. Capillary films play a key role in evaporation, often two-stage evaporation (Lehmann *et al*., 2008; Shokri *et al*., 2009; Shokri and Or, 2011). In the first stage, the evaporation rate was stable, approximately that of saturated soil. The rate of evaporation shifts to the second stage, where it declines dramatically when continuous drying increases the drying front depth to reach a characteristic length. The transition from the first to the second stages showed the disappearance or disconnection of the films that were originally connected to the soil surface.

Moreover, if the soil is hydrophobic and air becomes the wetting phase, the mechanisms of water entrapment and the retention of old water will differ, as water films will not develop. In this scenario, the non-wetting liquid-water-is more prone to becoming trapped in pore bodies as it gets snapped off by the pore throats it passes through (Tsao *et al*., 2020; Lake, 1989). Besides, the non-wetting phase tends to be squeezed out of small pores (*e.g*., pore throats) when the wetting phase invades (Tsao *et al*., 2020; Lake, 1989). In our experiment, if alcohol acts as the non-wetting phase and air as the wetting phase, the residual liquid will likely accumulate in pore bodies, surrounded by narrow pore paths (*i.e*., pore throats) after being displaced by air. When alcohol re-enters the porous media, capillary forces at the pore throats may impede its flow, causing it to move through large pore paths (preferential flows). As a result, the old liquid might not come into contact with the new liquid, potentially leading to more residual liquid remaining after each invasion event. This low wetting, even in the case of nonwetting liquid, may result in a higher retention of the old liquid, while the wetting liquid could wash out more of the old liquid.

4. CONCLUSIONS

We explored the interaction between new and old wetting liquids and the role of wetting films in this process by conducting grain-based micromodel experiments. After the drainage step, the wetting liquid became trapped in tight grain regions with small pore sizes, thereby influencing the remaining liquid saturation after evaporation. Interestingly, we found that rather than the initial old liquid content, the presence of a liquid film coating on grains played a crucial role in determining the entrapment of the pure old liquid. Film development facilitated the connection between the new and old liquids, enhancing air displacement in the pores and reducing the likelihood of air bubble formation. Conversely, weak film development resulted in increased air bubble entrapment, enhancing the separation of new and old liquids.

Previous studies have indicated that soil often exhibits partial wettability, particularly at a low water content. Under partial-wetting conditions, we demonstrated that a high contact angle resulted in weak film development and enhanced air entrapment. This partial wettability could enhance the separation of new and old water, highlighting the importance of considering the soil surface chemistry and wetting film development in future studies on new and old water interactions. Furthermore, in addition to the trapped pure old wetting liquid pockets, the mixing processes between the old and new liquids controlled the mass transport of the old liquid. Investigations into the effects of mixing processes on the old and new water interactions are required.

Conflicts of Interest: The authors declare that they have no known competing financial interests or personal relationships that could have appeared to influence the work reported in this paper.

5. REFERENCES

Berkowitz, B., 2014. Interchange of infiltrating and resident water in partially saturated media. In: Transport and Reactivity of Solutions in Confined Hydrosystems pp. 55-66: Springer. https://doi.org/10.1007/978-94-007-7534-3_5

Bico, J., Quéré, D., 2003. Precursors of impregnation. Europhys Lett. 61(3), 348-353. https://doi.org/10.1209/epl/i2003-00196-9

Bodas, D., Khan-Malek, C., 2006. Formation of more stable hydrophilic surfaces of PDMS by plasma and chemical treatments. Microelectron Eng. 83(4), 1277-1279. https://doi.org/10.1016/j.mee.2006.01.195

Brooks, J.R., Barnard, H.R., Coulombe, R., McDonnell, J.J., 2010. Ecohydrologic separation of water between trees and streams in a Mediterranean climate. Nat. Geosci. 3(2), 100-104. https://doi.org/10.1038/ngeo722

Chaudhury, M.K., Whitesides, G.M., 1991. Direct measurement of interfacial interactions between semispherical lenses and flat sheets of poly (dimethylsiloxane) and their chemical derivatives. Langmuir 7(5), 1013-1025. https://doi.org/10.1021/la00053a033

Chaudhury, M.K., Whitesides, G.M., 1992. Correlation between surface free energy and surface constitution. Science 255(5049), 1230-1232. https://doi.org/10.1126/science.255.5049.1230

Concus, P., Finn, R., 1969. On the behavior of a capillary surface in a wedge. Proc. National Academy of Sciences of the United States of America 63(2), 292. https://doi.org/10.1073/pnas.63.2.292

Concus, P., Finn, R., 1974. On capillary free surfaces in the absence of gravity. Acta Mathematica 132, 177-198. https://doi.org/10.1007/BF02392113

Dekker, L.W., Oostindie, K., Ritsema, C.J., 2005. Exponential increase of publications related to soil water repellency. Soil Res. 43(3), 403-441. https://doi.org/10.1071/SR05007

Dekker, L.W., Ritsema, C.J., 2000. Wetting patterns and moisture variability in water repellent Dutch soils. J. Hydrol. 231-232, 148-164. https://doi.org/10.1016/S0022-1694(00)00191-8

Doerr, S.H., Thomas, A.D., 2000. The role of soil moisture in controlling water repellency: new evidence from forest soils in Portugal. J. Hydrol. 231-232, 134-147. https://doi.org/10.1016/S0022-1694(00)00190-6

Fan, L.T., Yuan, X., Zhou, C.X., Zeng, A.W., Yu, K.T., Kalbassi, M., *et al*., 2011. Contact Angle of Ethanol and n-Propanol Aqueous Solutions on Metal Surfaces. Chem. Eng. Technol. 34. https://doi.org/10.1002/ceat.201000474

Finkenbiner, C.E., Good, S.P., Renée Brooks, J., Allen, S.T., Sasidharan, S., 2022. The extent to which soil hydraulics can explain ecohydrological separation. Nat Commun. 13(1), 6492. https://doi.org/10.1038/s41467-022-34215-7

Geistlinger, H., Ding, Y., Apelt, B., Schlüter, S., Küchler, M., Reuter, D., *et al*., 2019. Evaporation study based on micromodel experiments: Comparison of Theory and Experiment. Water Resour Res. 55(8), 6653-6672. https://doi.org/10.1029/2018WR024647

Gouet-Kaplan, M., Berkowitz, B., 2011. Measurements of interactions between resident and infiltrating water in a lattice micromodel. Vadose Zone J. 10(2), 624-633. http://dx.doi.org/10.2136/vzj2010.0103

Gouet-Kaplan, M., Tartakovsky, A., Berkowitz, B., 2009. Simulation of the interplay between resident and infiltrating water in partially saturated porous media. Water Resour Res. 45(5), n/a-n/a. http://dx.doi.org/10.1029/2008WR007350

Hsu, S.-Y., Zhang, Z.-Y., Tsao, C.-W., 2017. Thermoplastic micromodel investigation of two-phase flows in a fractured porous medium. Micromachines 8(2), 38. https://www.mdpi.com/2072-666X/8/2/38

Huang, Q.Z., Huang, J.C., Tsao, C.W., Hsu, S.Y., 2023. Pore doublet micromodel experiments of evaporation influence on pre-event water entrapment and pre-event and event water interaction. Adv. Water Resour. 177. https://doi.org/10.1016/j.advwatres.2023.104464

Horton, J.H., Hawkins, R.H., 1965. Flow path of rain from the soil surface to the water table. Soil Sci. 100(6): 377-383. https://journals.lww.com/soilsci/fulltext/1965/12000/flow_path_of_rain_from_the_soil_surface_to_the.1.aspx

Kirchner, J.W., Feng, X., Neal, C., 2000. Fractal stream chemistry and its implications for contaminant transport in catchments. Nature 403(6769), 524-527. https://doi.org/10.1038/35000537

Lake, L.W., 1989. Enhanced Oil Recovery, Prentice Hall, Englewood Cliffs, New Jersey, USA.

Lamorski, K., 2017. X-ray computational tomography facility. Institute of Agrophysics PAS. http://tomography.ipan.lublin.pl

Lehmann, P., Assouline, S., Or, D., 2008. Characteristic lengths affecting evaporative drying of porous media. Phys. Rev. E. 77(5), 056309. https://link.aps.org/doi/10.1103/PhysRevE.77.056309

Liu, Y., Jeng, D.-S., 2019. Pore structure of grain-size fractal granular material. Materials 12(13), 2053.

Ma'shum, M., Farmer, V., 1985. Origin and assessment of water repellency of a sandy South Australian soil. Soil Res. 23(4), 623-626.

Mata, A., Fleischman, A.J., Roy, S., 2005. Characterization of polydimethylsiloxane (PDMS) properties for biomedical micro/nanosystems. Biomed Microdevices 7(4), 281-293.

Oerter, E.J., Bowen, G., 2017. In situ monitoring of H and O stable isotopes in soil water reveals ecohydrologic dynamics in managed soil systems. Ecohydrology 10(4), e1841. https://doi.org/10.1002/eco.1841

Radolinski, J., Pangle, L., Klaus, J., Stewart, R.D., 2021. Testing the 'two water worlds' hypothesis under variable preferential flow conditions. Hydrol Process. 35(6), e14252. https://doi.org/10.1002/hyp.14252

Ritsema, C.J., Dekker, L.W., 2012. Soil water repellency: Occurrence, consequences, and amelioration. Elsevier.

Roper, M., Davies, S., Blackwell, P., Hall, D., Bakker, D., Jongepier, R., *et al*., 2015. Management options for water-repellent soils in Australian dryland agriculture. Soil Res. 53(7), 786-806.

Shao, G., Wu, J., Cai, Z., Wang, W., 2012. Fabrication of elastomeric high-aspect-ratio microstructures using polydimethylsiloxane (PDMS) double casting technique. Sens. Actuator A-Phys. 178, 230-236. https://doi.org/10.1016/j.sna.2012.01.034

Shokri, N., Lehmann, P., Or, D., 2009. Characteristics of evaporation from partially wettable porous media. Water Resour. Res. 45(2). https://doi.org/10.1029/2008WR007185

Shokri, N., Or, D., 2011. What determines drying rates at the onset of diffusion controlled stage-2 evaporation from porous media? Water Resour Res. 47(9).

Sklash, M., Stewart, M., Pearce, A., 1986. Storm runoff generation in humid headwater catchments: 2. A Case study of hillslope and low-order stream response. Water Resour. Res. 22(8),1273-1282.https://doi.org/10.1029/WR022i008p01273

Smith, W., Crane, M.D., 1930. The Jamin effect in cylindrical tubes. J. Am. Chem. Soc. 52(4), 1345-1349.

Tsao, C.-W., Huang, Q.-Z., You, C.-Y., Hilpert, M., Hsu, S.-Y., Lamorski, K., *et al*., 2020. The effect of channel aspect ratio on air entrapment during imbibition in soil-on-a-chip micromodels with 2D and 2.5 D pore structures. Lab on Chip. https://doi.org/10.1039/D0LC01029D

Tschapek, M., 1984. Criteria for Determining the hydrophilicity-hydrophobicity of Soils. Zeitschrift für Pflanzenernährung und Bodenkunde, 147(2), 137-149. https://onlinelibrary.wiley.com/doi/abs/10.1002/jpln.19841470202

Turton, D.J., Barnes, D.R., Jr., de Jesus Návar, J., 1995. Old and new water in subsurface flow from a forest soil block. J. Environ. Quality 24, 139-146. https://doi.org/10.2134/jeq1995.00472425002400010020x

Uchida, T., Tromp-van Meerveld, I., McDonnell, J.J., 2005. The role of lateral pipe flow in hillslope runoff response: an intercomparison of non-linear hillslope response. J. Hydrol. 311(1), 117-133. https://doi.org/10.1016/j.jhydrol.2005.01.012

Valat, B., Jouany, C., Riviere, L.M., 1991. Characterization of the wetting properties of air-dried peats and composts. Soil Sci. 152(2), 100-107.

Vorhauer, N., Wang, Y.J., Kharaghani, A., Tsotsas, E., Prat, M., 2015. Drying with formation of capillary rings in a model porous medium. Transp. Porous Media 110(2), 197-223. https://doi.org/10.1007/s11242-015-0538-1

Wang, Y.-L., Huang, Q.-Z., Hsu, S.-Y., 2023. The displacement of the resident wetting fluid by the invading wetting fluid in porous media using direct numerical simulation. Water 15(14), 2636. https://www.mdpi.com/2073-4441/15/14/2636

Yu, Y.-S., Wang, M.-C., Huang, X., 2017. Evaporative deposition of polystyrene microparticles on PDMS surface. Sci. Rep. 7(1), 1-9. https://www.nature.com/articles/s41598-017-14593-5